Korea-Australia Rheology Journal
Vol. 17, No. 4, December 2005 pp. 207-215

Microflow of dilute colloidal suspension in narrow channel of microfluidic-chip under Newtonian fluid slip condition

Myung-Suk Chun*, Tae Seok Lee and Kangtaek Lee[1]
Complex Fluids Research Lab., Korea Institute of Science and Technology (KIST), PO Box 131, Cheongryang, Seoul 130-650, South Korea
[1]Dept. of Chemical Eng., Yonsei University, Seodaemun-gu, Seoul 120-749, South Korea
(Received August 31, 2005; final revision received November 8, 2005)

Abstract

We present a finite difference solution for electrokinetic flow in rectangular microchannels encompassing Navier's fluid slip phenomena. The externally applied body force originated from between the nonlinear Poisson-Boltzmann field around the channel wall and the flow-induced electric field is employed in the equation of motion. The basic principle of net current conservation is applied in the ion transport. The effects of the slip length and the long-range repulsion upon the velocity profile are examined in conjunction with the friction factor. It is evident that the fluid slip counteracts the effect by the electric double layer and induces a larger flow rate. Particle streak imaging by fluorescent microscope and the data processing method developed ourselves are applied to straight channel designed to allow for flow visualization of dilute latex colloids underlying the condition of simple fluid. The reliability of the velocity profile determined by the flow imaging is justified by comparing with the finite difference solution. We recognized the behavior of fluid slip in velocity profiles at the hydrophobic surface of polydimethylsiloxane wall, from which the slip length was evaluated for different conditions.

Keywords : microfluidic-chip, colloidal suspension, fluid slip, electrokinetic flow, particle streak, polydimethylsiloxane channel

1. Introduction

Newtonian fluid slip at hydrophobic surfaces has favorably been observed at the length scale of micrometers. Further, hydrophobic materials have become increasingly attractive for use in fabrication of micropatterned devices. Thus, an understanding of the physics of either microfluids or micro-rheology involving electrokinetic phenomena and fluid slip is needed for design and operation of microfluidic flow in micro-electro mechanical system (MEMS) devices (Karniadakis and Beskok, 2003; Tretheway and Meinhart, 2003; Tretheway and Meinhart, 2004).

In most of the experiments probing slip, a slip length is or can be inferred from measurements (Lauga and Stone, 2003). A common definition of a slip length (or sometimes, a slip coefficient) β at a rigid boundary, with unit normal vector $\boldsymbol{n}$ directed into the fluid, linearly relates the velocity at the wall to the wall shear strain rate

$$\boldsymbol{v} = \beta \boldsymbol{n} \cdot [(\nabla \boldsymbol{v}) + (\nabla \boldsymbol{v})^T] \quad (1)$$

where β is assumed to be a material parameter. This relation was first proposed by Navier in 1823 for liquids and was also rigorously derived by Maxwell in 1879 in the case of gases. As shown in Fig. 1, the slip length is the local equivalent distance below the solid surface at which the no-slip boundary condition would be satisfied if the flow field were extended linearly outside of the physical domain.

On the contrary, the absence of slip would provide an increased drag on the flow due to the effect of electric double layer (EDL) in charged microchannels, resulting in an apparent viscosity which is higher than the true fluid viscosity. This is referred to as the electroviscous effect (Li, 2001; Chun and Kwak, 2003). Both the electroviscous and fluid slip phenomena should be examined simultaneously since they have

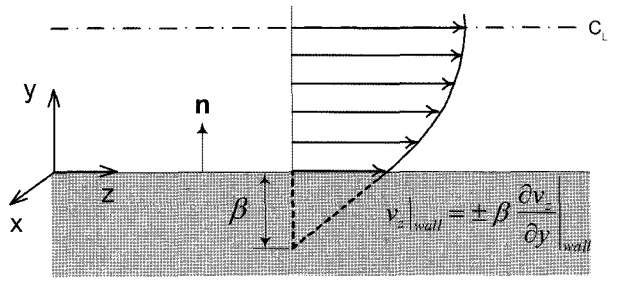

Fig. 1. Schematic of fluid slip at hydrophobic surface.

*Corresponding author: mschun@kist.re.kr

countereffects on fluid flow in microchannels.

Many studies have contributed to the fluid slip. Watanabe *et al.* (1999) observed water slippage in an acrylic-resin-coated pipe and obtained a 14% drag reduction. Zhu and Granick (2001) addressed fluid motion adjacent to smooth surfaces exhibiting some manifestations of microscopic slip. Tretheway and Meinhart (2002) measured the velocity profile of water flowing through the hydrophobic treated microchannel and observed a 1 μm slip length. However, so far there have been a very limited number of studies of electrokinetic flow in microchannels or microcapillaries that exhibits results consistent with fluid slip at the solid boundary.

In this study, we present numerical solutions for laminar electrokinetic flow with Navier's slip condition in rectangular channels. The fluid velocity is obtained with variations of EDL thickness as well as slip length employing the finite difference method. Theoretical results regarding the velocity enhancement (i.e., reciprocal electroviscous effect) and friction factor are provided for different situations. The velocity profile of dilute latex suspension in polydimethylsiloxane (PDMS) based microfluidic-chip is determined by applying the particle streak velocimetry (PSV). The PSV adopted in this study involves recording particle displacements in a single image over a period of time, in which sparse quantitative particle velocity data may be obtained as reported in the literature (Taylor and Yeung, 1993; Oddy *et al.*, 2001; Stone *et al.*, 2004). The slit-like channel has been fabricated by designing high-aspect-ratio of the channel depth to the width that practically allows a parallel uniaxial flow. To guarantee the accuracy of our experiments, each velocity profile determined by the PSV is compared with simulation results. A microchannel made of walls of dissimilar materials results in the asymmetric flow characteristic. We examine the behavior of the Newtonian fluid slip encountered in a hydrophobic PDMS wall with variations of the surface potential acquired with the change of suspension pH.

2. Theoretical consideration of electrokinetic microflow with fluid slip

2.1. Flow field coupled with electrokinetic streaming potential

We consider a situation for pressure-driven and steady-state electrokinetic flow through a uniformly charged straight rectangular microchannel. Cartesian coordinates are introduced, where z is the distance along the axis of a microchannel. The development of the electrokinetic flow equation extends those of previous works (Rice and Whitehead, 1965; Karniadakis and Beskok, 2003) to symmetric electrolytes in which the mobilities of anions and cations may individually be specified.

For incompressible laminar flow, the velocity of ionic fluid is expressed as $\boldsymbol{v} = [0, 0, v_z(x, y)]$, the pressure $p = p(z)$, and the flow-induced electric field $\boldsymbol{E} = [0, 0, E_z(z)]$. Neglecting gravitational forces, the body force per unit volume ubiquitously caused by the z-directional action of flow-induced electric field E_z on the net charge density ρ_e can be written as $F_z = \rho_e E_z$ (Yang and Li, 1997; Chun *et al.*, 2005). The E_z is defined by the flow-induced streaming potential ϕ as $E_z = -d\phi(z)/dz$. With these identities, the Navier-Stokes equation reduces to

$$\eta\left[\frac{\partial^2 v_z}{\partial x^2}+\frac{\partial^2 v_z}{\partial y^2}\right]=\frac{dp}{dz}-\rho_e E_z. \tag{2}$$

where η is the fluid viscosity. Based on Eq. (1), the slip boundary condition at the hydrophobic surface is commonly expressed as $v_z|_{wall} = \pm\beta(\partial v_z/\partial y)|_{wall}$ in Fig. 1, from which each boundary condition applied to $v_z(x, y)$ yields

$$v_z(x,y)\big|_{x=0}=\beta_L\left.\frac{\partial v_z(x,y)}{\partial x}\right|_{x=0} \quad \text{at } x=0, \tag{3a}$$

$$v_z(x,y)\big|_{x=W}=-\beta_R\left.\frac{\partial v_z(x,y)}{\partial x}\right|_{x=W} \quad \text{at } x=W, \tag{3b}$$

$$v_z(x,y)\big|_{y=0}=\beta_B\left.\frac{\partial v_z(x,y)}{\partial y}\right|_{y=0} \quad \text{at } y=0, \tag{3c}$$

$$v_z(x,y)\big|_{y=H}=-\beta_T\left.\frac{\partial v_z(x,y)}{\partial y}\right|_{y=H} \quad \text{at } y=H. \tag{3d}$$

Since the velocity becomes maximum at the center of the channel, the sign of the velocity gradient changes into negative along the axis. Hence, a right-hand side of Eqs. (3b) and (3d) has positive value. The no-slip boundary condition is easily applied by setting $\beta = 0$.

When the charged surface is in contact with an electrolyte, the electrostatic charge would influence the distribution of nearby ions. Consequently, an electric field is established and the positions of the individual ions in solution are replaced by the mean concentration of ions. For a rectangular channel, the nonlinear Poisson-Boltzmann (P-B) equation governing the electric potential field is given as (Probstein, 1994)

$$\frac{\partial^2 \Psi}{\partial x^2}+\frac{\partial^2 \Psi}{\partial y^2}=\kappa^2 \sinh \Psi. \tag{4}$$

Here, the dimensionless electric potential Ψ denotes $Ze\psi/kT$ and the inverse EDL thickness (namely, inverse Debye thickness) κ is defined by $\kappa=\sqrt{2n_b Z_i^2 e^2/\varepsilon kT}$, where n_b is the electrolyte ionic concentration in the bulk solution at the electroneutral state, Z_i the valence of type i ions, e the elementary charge, ε the dielectric constant, and kT the Boltzmann thermal energy. The n_b (1/m^3) equals to the product of the Avogadro's number N_A (1/mol) and bulk electrolyte concentration (mM). The Boltzmann distribution of the ionic concentration of type i (i.e., $n_i = n_b \exp(-Z_i e\psi/kT)$) provides a local charge density $Z_i e n_i$.

We determine the net charge density ρ_e ($\equiv\Sigma_i Z_i e n_i = Ze(n_+ - n_-)$), as follows

$$\rho_e = Zen_b[\exp(-\Psi)-\exp(\Psi)] = -2Zen_b\sinh\Psi. \quad (5)$$

Substituting Eq. (5) into Eq. (2) yields

$$\frac{\partial^2 v_z}{\partial x^2}+\frac{\partial^2 v_z}{\partial y^2} = -\frac{1}{\eta}\frac{\Delta p}{L}+\frac{2Zen_b\sinh\Psi}{\eta}\frac{\Delta\phi}{L} \quad (6)$$

where L means channel length, $\Delta p = p_0 - p_L$, and $\Delta\phi = \phi_0 - \phi_L$. In Eq. (6), the fluid velocity is coupled with the flow-induced streaming potential ϕ. Once the channel wall is uncharged (i.e., inert), the velocity profile accompanying slip effect can be analytically determined from the Stokes equation of motion given by $\eta\nabla^2\boldsymbol{v} = \nabla p$.

In order to analyze the velocity profile, the net current conservation is applied in the microchannel taking into account the Nernst-Planck equation. This equation describes the transport of ions in terms of convection and migration resulting from the pressure difference and electric potential gradient, respectively. Ions in the mobile region of the EDL are transported through the channel, commonly causing the electric convection current (i.e., streaming current) I_S. The accumulation of ions provides the streaming potential difference $\Delta\phi$ ($= E_z L$). This field causes the conduction current I_C to flow back in the opposite direction. In this case, the net current I consists of I_S and I_C, and it should be zero at the steady state, viz. $I \equiv I_S + I_C = 0$ (Werner *et al.*, 1998). After complicated procedures, the streaming potential can finally be derived as follows

$$\Delta\phi = \frac{L\int_0^H\int_0^W \rho_e(x,y)v_z(x,y)dxdy}{\left\{\begin{array}{c} W(\lambda_{s,T}+\lambda_{s,B})+H(\lambda_{s,R}+\lambda_{s,L}) \\ +Z^2e^2N_A\int_0^H\int_0^W[K_+n_+(x,y)+K_-n_-(x,y)]dxdy \end{array}\right\}}. \quad (7)$$

Here, λ_s indicates the specific surface conductivity depending on the material property of channel wall and K_i is the mobility of ion species i defined as its velocity in the direction of an electric field of unit strength. The subscripts + and – of the ionic number concentration n_i denote the cations and the anions, respectively.

2.2. Finite difference analysis

Basic procedures of the present finite difference method are analogous to the previous work (Chun *et al.*, 2005). To obtain the solution of the nonlinear $P-B$ equation with the boundary conditions imposed as $\Psi = \Psi_{s,L}$ at $x = 0$, $\Psi = \Psi_{s,R}$ at $x = W$, $\Psi = \Psi_{s,B}$ at $y = 0$, and $\Psi = \Psi_{s,T}$ at $y = H$, the five-point central difference method is taken on the left-hand side of Eq. (4). The sinh Ψ on the right-hand side can be linearized as $\sinh\Psi^k_{l,m}+(\Psi^{k+1}_{l,m}-\Psi^k_{l,m})\cosh\Psi^k_{l,m}$, where k means the iteration index and the grid index l and $m = 1, 2, \ldots, N$. The finite difference form of the nonlinear $P-B$ equation becomes

$$\frac{\Psi^{k+1}_{l+1,m}-2\Psi^{k+1}_{l,m}+\Psi^{k+1}_{l-1,m}}{\Delta x^2}+\frac{\Psi^{k+1}_{l,m+1}-2\Psi^{k+1}_{l,m}+\Psi^{k+1}_{l,m-1}}{\Delta y^2}$$
$$= \kappa^2[\sinh\Psi^k_{l,m}+(\Psi^{k+1}_{l,m}-\Psi^k_{l,m})\cosh\Psi^k_{l,m}]. \quad (8)$$

Then, Eq. (8) is rewritten as

$$\Psi^{k+1}_{l-1,m}+\gamma\Psi^{k+1}_{l,m-1}-[2+2\gamma+(\kappa\Delta x)^2\cosh\Psi^k_{l,m}]\Psi^{k+1}_{l,m}+\gamma\Psi^{k+1}_{l,m+1}$$
$$+\Psi^{k+1}_{l+1,m} = (\kappa\Delta x)^2[\sinh\Psi^k_{l,m}-\Psi^k_{l,m}\cosh\Psi^k_{l,m}]. \quad (9)$$

where $\gamma = (\Delta x/\Delta y)^2$. Eq. (9) can be solved for $\Psi^{k+1}_{l,m}$ by successive under-relaxation iterative calculation, using the value of Ψ obtained in the k-th iteration. The electric potentials Ψ at four corners are dummy values, which do not affect the solution of the P-B equation. The electric potential is obtained from a series of algebraic equations expressed in a matrix form, and then the fluid velocity can be computed by solving Eq. (6) together with Eq. (7). For the velocity profile with relevant boundary conditions, a similar finite difference scheme represented as Eq. (9) is used again.

Illustrative computations are performed considering a fully developed flow of the aqueous electrolyte fluid in a 10 μm square microchannel with $\Delta p/L = 1.0$ bar/m. Here, γ is a unity because the square domain is divided into equal increments in the x and y directions. The grids of 101 × 101 meshes were built within the channel and the convergence criterion is given to satisfy the accuracy requirement. The dielectric constant ε is given as a product of the dielectric permittivity of a vacuum ($= 8.854 \times 10^{-12}$ C^2/J·m) and the relative permittivity for aqueous fluid (= 80). The fluid viscosity is taken as 1.0×10^{-3} kg/m·sec, at room temperature. For 1:1 type electrolyte, the EDL thickness κ^{-1} (nm) is expressed as [fluid ionic concentration (M)]$^{-1/2}$/3.278. The EDL thicknesses correspond to 9.7, 96.5, and 965 nm for bulk electrolyte concentrations of 1.0, 10^{-2}, and 10^{-4} mM, where thinning of the EDL means the decrease of electrostatic repulsion.

Fig. 2 demonstrates how the velocity changes with variations of the EDL thickness (i.e., κR_h, where R_h is the hydraulic radius) as well as the slip length. The dimensionless surface potential Ψ is fixed as 2, equivalent to $2kT/e = 25.69$ mV. Velocity decreases with decreasing inverse EDL thickness, meaning an increase of the electrokinetic interaction due to electrostatic repulsion. The velocity is enhanced in accordance with increasing of the slip length β_L, in which the asymmetric condition of slip length is applied. We estimate the velocity enhancement from the ratio of the average velocity in a charged channel to that in an inert one. If the apparent viscosity η_a stands for the fluid viscosity of charged case, the velocity enhancement corresponds to the inverse of electroviscous effect, as given

$$\frac{\langle v_z\rangle}{\langle v_z\rangle_{inert}} = \frac{\eta_{inert}}{\eta_a} \quad (10)$$

As shown in Fig. 3, the presence of EDL retards flow rate,

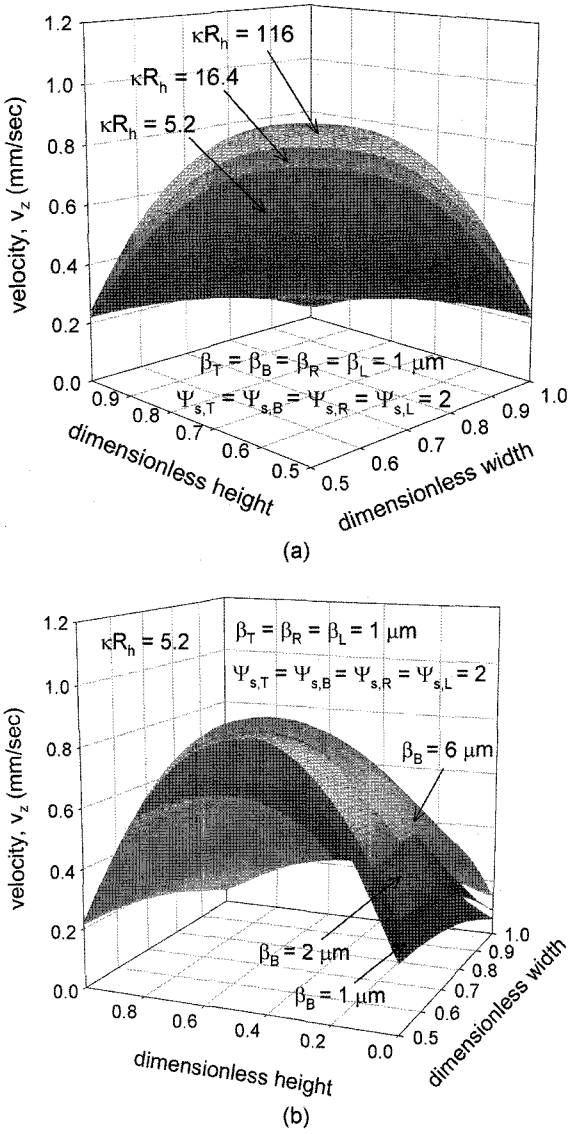

Fig. 2. Simulation results of velocity profile in hydrophobic rectangular microchannel for influence of (a) electric double layer thickness, and (b) slip length, where $R_h = 5$ μm.

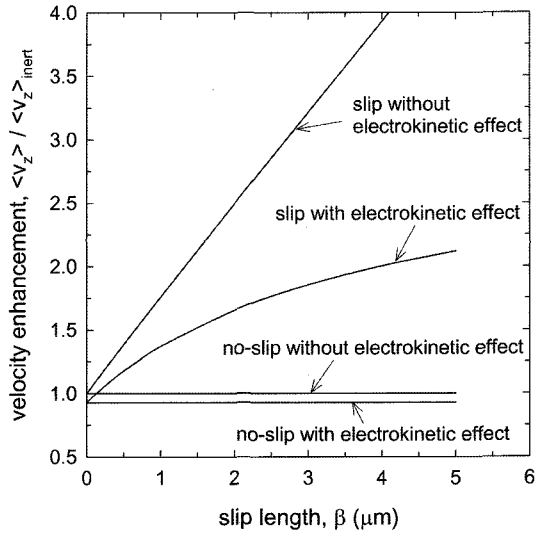

Fig. 3. Effect of fluid slip and electric double layer on velocity enhancement with variations of slip length, where $\Psi_s = 2$, $\kappa R_h = 5.2$, and $R_h = 5$ μm.

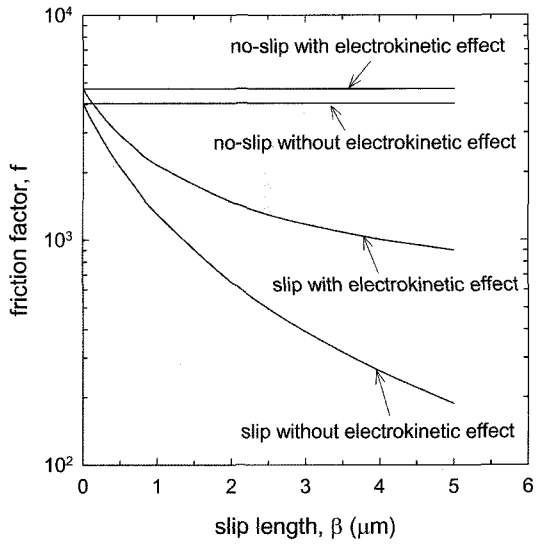

Fig. 4. Effect of fluid slip and electric double layer on friction factor with variations of slip length, where $\Psi_s = 2$, $\kappa R_h = 5.2$, and $R_h = 5$ μm.

while fluid slip induces a higher flow velocity. The EDL effect causes the observed velocity to be different from the case of no-slip without electrokinetic effect and can results in the apparent viscosity. A higher apparent viscosity would be predicted if fluid slip is neglected. The friction factor is a proportionality constant between the force that would be exerted by the motion of fluid and characteristic kinetic energy along the channel length. It can be given as a function of the Re and the system parameter, yielding

$$f = -\frac{R_h}{2}\frac{dp/dz}{\rho\langle v_z\rangle^2/2} \tag{11}$$

where ρ is the fluid density. Fig. 4 shows opposite behavior observed in Fig. 3. The friction factor is reduced by fluid slip effect, whereas it is increased with the EDL effect.

3. Flow visualization experiments

3.1. PDMS microfluidic-chip fabrication

The PDMS has been widely used in the microfluidics as a microfabrication material due to its simple process and low cost when compared to traditional etching and bonding approaches. Chip fabrication procedures are similar to previously published work (Chun and Lee, 2005). Channel design was performed with AutoCAD-2004, and a high-

resolution chromium mask supplied by photomask manufacturer (Advance Reproductions Corporation, MA) was prepared to minimize the surface roughness of the channel. The microchannel is a slit 2.6 cm long by 80 μm wide and 800 μm depth. A negative-tone UV photoresist (PR) of SU8-50 (MicroChem, MA) is used to generate the master on a silicon wafer (LG-Siltron Inc., 4" Prime P-100, Korea). The PR is spin-coated on a pretreated wafer, subjecting to a Piranha cleaning (H_2SO_4:H_2O_2 = 3:1, volume ratio). The spin speed of 1100 rpm for a total of 30 sec is set to obtain the 80 μm height, which becomes the channel width later.

Soft bake follows as consisting of the pre-bake at 65°C for 5 min and the soft-bake at 95°C for 30 min. The negatively-patterned PR is obtained through the UV exposure with aligner (Karl Süss MA6, Germany), where the power of 20 mW/cm^2 is applied with i-line wavelength of 365 nm. Following exposure, a post exposure bake (PEB) is performed to selectively cross-link the exposed portions of the mask. The PEB also contains a two-step procedure; the PEB I at 65°C for 1 min and the PEB II at 95°C for 10 min. We have the wafer cool down slowly to room temperature, and unexposed PR is removed by dissolving with the developer (MicroChem SU8 Developer, MA) for 20 min with mild shaking. A master mold containing negatively-patterned PR is remained, after rinsing the wafer with isopropyl alcohol and deionized-water.

The lateral side of the replica becomes a lid of the slit-like channel, where the thickness of the lid is desirably less than 1 mm to permit optical access for flow imaging. The edge of the wafer mold should be cut and a side wall stands at the cutting surface. To produce a replica, PDMS (Sylgard 184, Dow Corning, MI) is mixed with the curing agent in the volume ratio of 10:1, and poured on the wafer mold (McDonald and Whitesides, 2002). In this study, preliminary tubing is adhered to and stand at the corresponding inlet and outlet reservoirs of 1.2 mm diameter in the master mold, before the pouring. After bubbles are eliminated at 80 Torr for 1 hour evacuation, the PDMS is cured at 80°C for 2 hours in 1 atm. The PDMS replica is peeled from the master, and then the replica is washed by sonication together with the glass coverslip (Marienfeld Micro Slides, Germany) using methanol. Applying the reactive ion etching, both surfaces activated by O_2 plasma were sealed each other. To make PDMS-glass chip, it is required to put the activated surface of PDMS onto that of glass for about 2 – 3 hours for stronger adhesion. Instead of the bonding with the glass cover, another type of microfluidic-chip having PDMS-PDMS channel was also fabricated. In Fig. 5, the high-aspect-ratio (*i.e.*, 10:1) of channel depth H to channel width W makes the uniaxial flow.

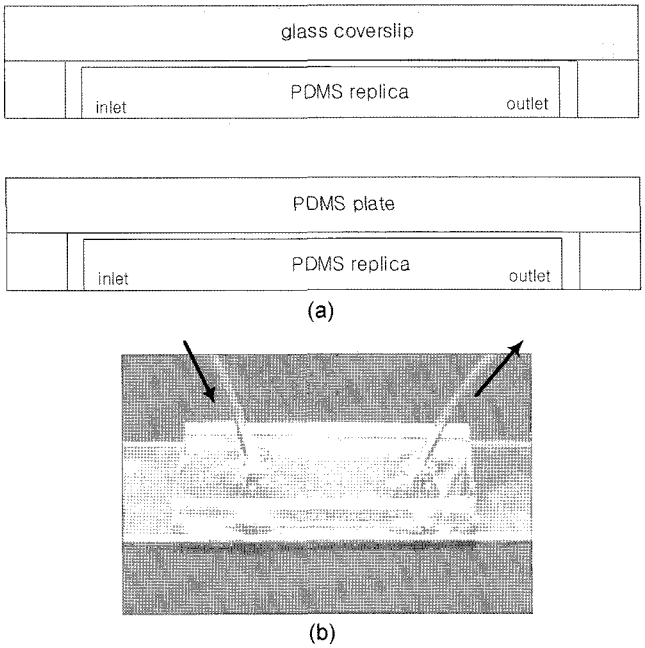

Fig. 5. Microfluidic-chip with high-aspect-ratio microchannel, (a) top view of the channel confined with PDMS-glass and PDMS-PDMS wall, and (b) PDMS replica bonded with glass coverslip.

3.2. Microflow system and fluorescent microscope

The motion of the bulk fluid in particle-based flow velocimetry is inferred from the observed velocity of marker particles. Seeding of the flow field was achieved with fluorescent polystyrene latex (Sigma L-5280, MO) of radius 1.05 μm and density of 1.003. The order of settling velocity is very small, so the gravity effect is negligible. Latex colloids were dispersed with extremely dilute concentration of 0.48 ppm. Deionized ultrafiltered water was used, and the ionic concentration of suspension was maintained as 0.5 mM KCl electrolyte with κ^{-1} of 13.6 nm. Nonionic surfactant of Triton X-100 at 0.4 g/liter was used to prevent the aggregation of latexes. The imaging system and experimental setup are shown in Fig. 6. The suspension was carefully supplied to the chip by syringe pump (Cole-Parmer 7600 Series, IL), and a high-precision pressure gauge with ±0.1% FS accuracy (FD2000, Honeywell Sensotec, OH) measured the pressure drop across the channel. The volumetric flow rate was measured by electronic balance (Mettler-Toledo AG, Switzerland) with accuracy of 1.0 mg.

In the stereomicroscope (SV-11, Carl Zeiss, Germany) equipped with fluorescent illuminator, it has a zoom range of 0.6x to 6.6x with a numerical aperture of 0.085 and objective lens (Achromat S 2.5x). Illumination was provided by C FL S illuminator having a super-pressure mercury lamp spectrally filtered with a fluorescent filter cube FITC system. Images were captured by a digital charge-coupled device (CCD) camera (Ultra-High Resolution AxioCam) having a basic resolution of 1300 × 1030 pixels

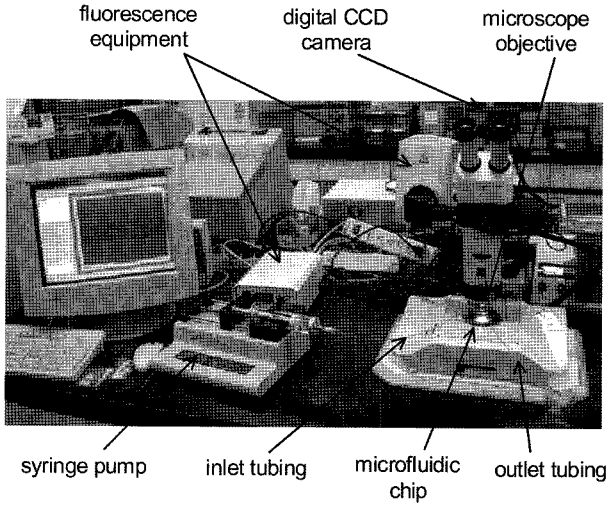

Fig. 6. Photograph of the experimental setup.

in color, with a digitization of 14 Bit/10 Mhz and a pixel size of 6.7 μm. Its spectral range is 300 – 1000 nm and the Peltier cooling integrates for up to 40 sec.

The view field and focal plane were adjusted to collect the image from the bulk region without the effect of upside PDMS wall onto the one-dimensional flow. The image observations were done 1.5 cm downstream of the entrance into the channel where the flow is fully developed. The exposure time was set to 200 ms. The transmitted-light was used to recognize the channel width, however, we depressed the band of emission light from the particles. The data from the CCD camera was fed to a monitor for real-time viewing and to a PC-based frame grabber for image acquisition, using the digital imaging software Axio-Vision 3.1. The image data consist of each pixel equivalent to the intensity of the light, where an image of particle streak is represented with green color. Data acquisition was accomplished by the image processing algorithm developed in our laboratory with implementing MATLAB (Mathworks, MA).

4. Experimental results

4.1. Microchannel surface characterization

Since surface roughness is to play an important role in boundary slip, we carried out the atomic force microscopy (AFM) imaging with variation of surface topography at nanoscale resolution using a Nanoscope III (Digital Instruments). For PDMS plate and PDMS replica, root mean square (RMS) roughness taken at different regions was estimated as 0.48 and 0.42 nm, respectively. This level of smoothness is sufficient not to generate no-slip. In Fig. 7, the values of contact angle measured by drop shape measuring system (DSA-10, Krüss GmbH, Hamburg) provide 54 and 99 deg for glass surface and PDMS plate, respectively. There is no difference between PDMS plate and PDMS replica.

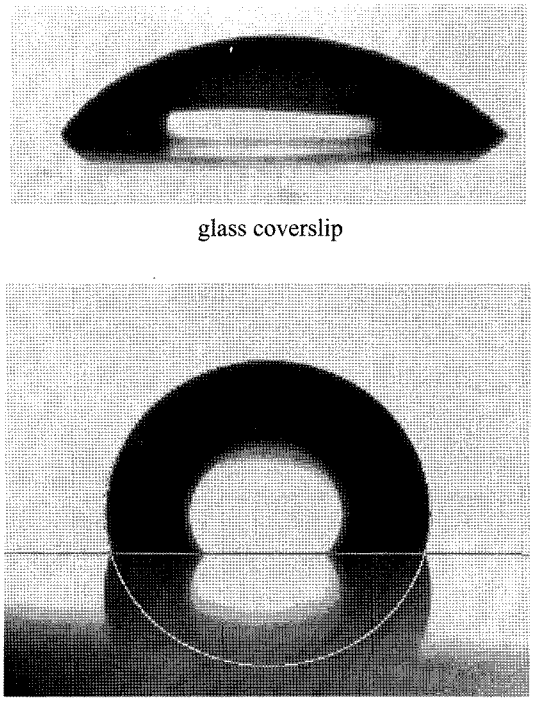

Fig. 7. Close-up view of contact angle.

The zeta potentials of each material used in this study were previously reported (Chun and Lee, 2005). Both the PDMS and the glass surfaces exhibit that the magnitude of the negative zeta potential increases with increasing the pH of suspension. The PDMS plate is negatively charged in above pH 4, but it is considered to be weakly charged as being due to lower magnitude of zeta potential. The glass surfaces are negatively charged likewise the PDMS plate, where its magnitude of zeta potential was greater about 20 mV than that of the PDMS. Long-range interactions between particle-to-particle as well as particle-to-wall are important especially in microfluidic system. The negative surface charges certainly minimize the affinity of the particles to adhere either to themselves or to the negatively-charged channel walls.

4.2. Velocity profile and slip length

Local particle velocities at each position were obtained. In order to guarantee the velocity profile of suspension determined by local particle velocities, the ratio of particle diameter d_p to channel width W should be small besides the condition of sufficiently dilute particle concentration. When the latex particle is suspended in a viscous fluid undergoing Poiseuille flow within the channel, both the particle slip velocity and the lateral migration velocity are inevitably presented. A buoyant

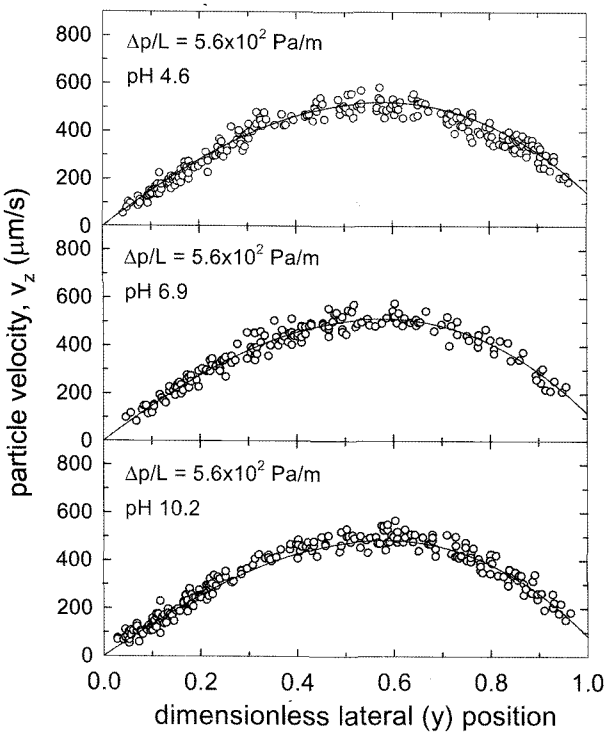

Fig. 8. Uniaxial velocity profile in slit-like channel of PDMS-glass microfluidic-chip for different pH at 0.5 mM KCl electrolyte fluid, where solid curves correspond to finite difference computation.

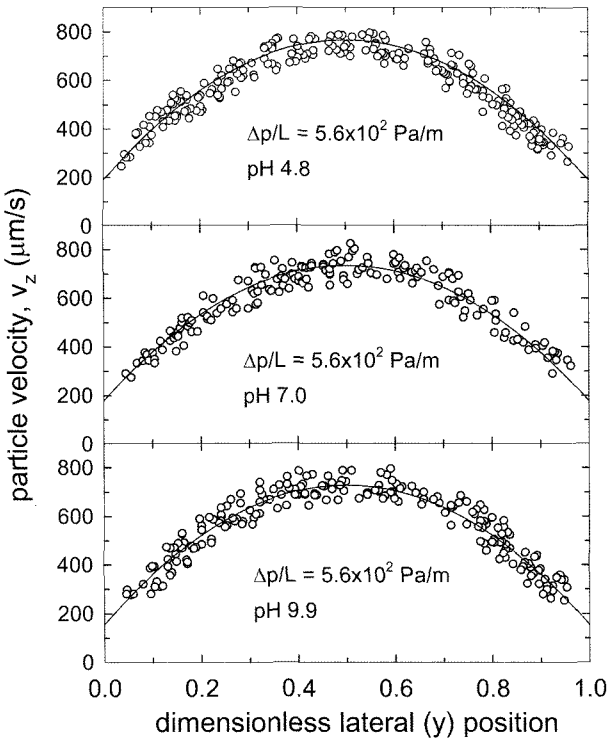

Fig. 9. Uniaxial velocity profile in slit-like channel of PDMS-PDMS microfluidic-chip for different pH at 0.5 mM KCl electrolyte fluid, where solid curves correspond to finite difference computation.

particle is carried by a velocity less than unperturbed fluid velocity occurred by the particle slip phenomena (Ho and Leal, 1974). The migration velocity is related to the hydrodynamic lateral force due to the particle inertia in bounded flows (Cox and Brenner, 1968; DosRamos and Silebi, 1989). Theoretical calculations conducting relevant equations reported in the literature show that, as the relative particle size decreases, both the particle slip and the lateral migration effects become almost disappeared. The d_p/W of 0.026 in this study is consistent with a regime neglecting these effects.

Fig. 8 shows the velocity profile obtained for different pH, meaning a change in the surface potentials of each channel wall. The glass wall corresponds to the left-side of x-axis and the PDMS wall corresponds to the right-side of x-axis. We found it is difficult to obtain reliable measurements closer to the wall because of the image noise associated with particle light scatter at the wall surface. Nonetheless, it is clearly recognized that a slip effect exists at the PDMS wall. PDMS surface is hydrophobic whereas the glass is hydrophilic, therefore, this inhomogeneous surface condition results in an asymmetric velocity profile in the PDMS-glass chip. As shown in Fig. 9, the measured velocity profile is represented by the slip velocity at both sides of the wall, allowing a symmetric view. Even though an explicit comparison is limited somewhat due to scattering data in Figs. 8 and 9, fair agreements can be seen between experiments and corresponding computational. It allows us to figure out the reliability of our flow visualization. We would point out that a decreasing trend of average velocity with increasing pH is slight, since the pH of suspension does not exhibit remarkable effects on the flow pattern in our condition.

In Figs. 8 and 9, the EDL thickness is very thin compared to the channel width as well as particle radius. Thus, the electrophoretic velocity of a single particle is obtained as $\varepsilon\zeta_p E_z/\eta$, where ζ_p is the zeta potential of the particle and E_z ($=\Delta\phi/L$) is the applied electric field (Probstein, 1994). The flow-induced streaming potential ϕ has quite small order of magnitude compared to the voltages commonly supplied in the case of electrophoresis as external power source. Accordingly, the effect of electrophoretic particle velocity is really negligible in this study.

It is possible to estimate the slip length analyzing the data points nearby the PDMS wall along the regressions. The wall slip velocity $v_z|_{wall}$ is decreased with increasing pH as found in Figs. 8 and 9. Fig. 10 shows that the slip length has an approximate trend to decrease as the pH increases causing the stronger electrokinetic effect. The variations of slip length at PDMS surface can be identified ranging

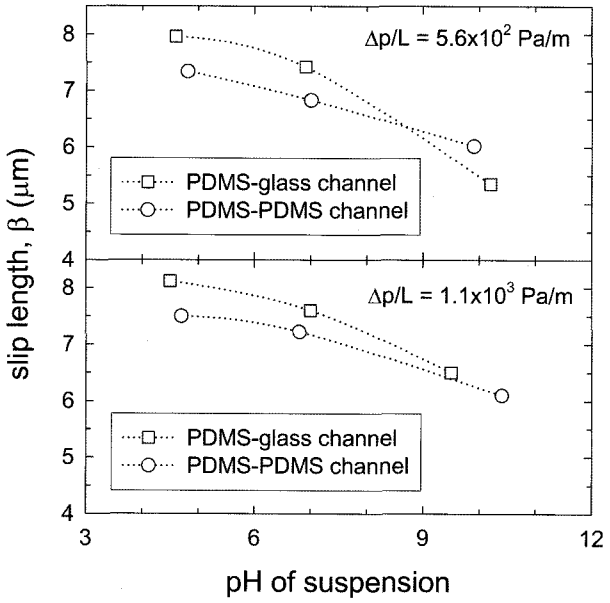

Fig. 10. The variation of the slip length for PDMS-glass and PDMS-PDMS channels for different suspension pH with pressure gradients of 5.6×10^2 Pa/m and 1.1×10^3 Pa/m.

about 5.5 to 8 μm, where the magnitude of β/W is of the order of what is summarized in the literature (Lauga and Stone, 2003). Although the slip length is almost independent on the pressure gradient, it seems observation of this independency is limited up to critical pressure gradient. Beyond this value, the slip length may change as Zhu and Granick (2002) have suggested.

5. Conclusions

In our theoretical model of electrokinetic flow in microchannels, the individual effect of each parameter can be analyzed, and micro-rheological results usefully provide design guidelines to control the transport behavior. It is evident that fluid slip at the wall and electrokinetic effect are both important and should be considered simultaneously. Newtonian fluid slip induces a larger flow velocity, which plays a contrary role to the electroviscous effect giving rise to a reduction in the flow. If the slip is absent, a higher apparent viscosity and a higher friction factor would be predicted.

Experimental observations provide reasonably benchmark data for the verification of attempting theoretical study for understanding of microflows and developing novel micro processes. Since particle streak images are suitable to get velocity profile information, fluorescent microscope experiments have been implemented to examine the electrokinetic microflow. Applying on a parallel uniaxial flow field, the velocity profile of dilute latex suspension was obtained in narrow channels of PDMS-glass as well as PDMS-PDMS chip. It is necessary to introduce a low ratio of particle size to channel width that removes the nature of both the particle slip and the lateral migration.

The validity of the velocity profile determined by flow visualization was justified by comparing with the computational results, where a good agreement was found. The wall slip velocity was observed at the hydrophobic surface of the PDMS wall, in which PDMS-PDMS channel resulted in a higher flow velocity than PDMS-glass one at the same condition. It is available to obtain the dependency of slip length on the suspension pH.

Nomenclatures

d_p	: diameter of particle [m]
E_z	: applied electric field in axial direction [V/m]
e	: elementary charge [C]
f	: friction factor [–]
H	: channel depth [m]
I	: net electric current [A]
I_C	: conduction current [A]
I_S	: streaming current, or convection current [A]
K	: mobility of ion species [mol·s/kg]
kT	: Boltzmann thermal energy [J]
L	: channel length [m]
N_A	: Avogadro's number [1/mol]
$\boldsymbol{n}$	: unit normal vector directed into the fluid [–]
n	: number concentration of ion species [1/m^3]
p	: hydraulic pressure [Pa]
R_h	: hydraulic radius [m]
v_z	: axial particle velocity [m/s]
W	: channel width [m]
x, y, z	: positional direction [m]
Z	: valence of ion species [–]

Greek Letters

β	: slip coefficient or slip length [m]
γ	: $(\Delta x/\Delta y)^2$ [–]
ε	: dielectric constant, or permittivity of the medium [C^2/J·m]
η	: fluid viscosity [Pa·s]
κ	: inverse EDL thickness [1/m]
λ_s	: specific surface conductivity [S]
ρ	: fluid density [kg/m^3]
ρ_e	: net charge density [C/m^3]
ϕ	: flow-induced streaming potential [V]
Ψ	: dimensionless electric potential [–]
ψ	: electric potential [V]

Subscripts

B	: bottom
L	: left
R	: right
T	: top

Acknowledgements

This work was supported by the Basic Research Funds (R01-2004-000-10944-0) from the Korea Science and Engineering Foundations (KOSEF). Authors wish to extend sincere gratitude to the staffs at the Micro-Nano Fabrication Center located in the KIST for valuable technical advice.

References

Chun, M.-S. and H.W. Kwak, 2003, Electrokinetic flow and electroviscous effect in a charged slit-like microfluidic channel with nonlinear Poisson-Boltzmann field, *Korea-Australia Rheology J.* **15**, 83.

Chun, M.-S., T.S. Lee and N.W. Choi, 2005, Microfluidic analysis on electrokinetic streaming potential induced by microflows of monovalent electrolyte solution, *J. Micromech. Microeng.* **15**, 710.

Chun, M.-S. and S. Lee, 2005, Flow imaging of dilute colloidal suspension in PDMS-based microfluidic chip using fluorescence microscopy, *Coll. Surf. A: Physicochem. Eng. Aspects* **267**, 86.

Cox, R.G. and H. Brenner, 1968, The lateral migration of solid particles in Poiseuille flow: I. Theory, *Chem. Eng. Sci.* **23**, 147.

DosRamos, J.G. and C.A. Silebi, 1989, An analysis of the separation of submicron particles by capillary hydrodynamic fractionation (CHDF), *J. Colloid Interface Sci.* **133**, 302.

Ho, B.P. and L.G. Leal, 1974, Inertial migration of rigid spheres in two-dimensional unidirectional flows, *J. Fluid Mech.* **65**, 365.

Karniadakis, G.E. and A. Beskok, 2003, Micro Flows: Fundamentals and Simulation, Springer-Verlag, New York.

Lauga, E. and H.A. Stone, 2003, Effective slip in pressure-driven Stokes flow, *J. Fluid Mech.* **489**, 55.

Li, D., 2001, Electro-viscous effects on pressure-driven liquid flow in microchannels, *Coll. Surf. A: Physicochem. Eng. Aspects* **195**, 35.

McDonald, J.C. and G.M. Whitesides, 2002, Poly(dimethylsiloxane) as a material for fabricating microfluidic devices, *Acc. Chem. Res.* **35**, 491.

Oddy, M.H., J.G. Santiago and J.C. Mikkelsen, 2001, Electrokinetic instability micromixing, *Anal. Chem.* **73**, 5822.

Probstein, R.F., 1994, *Physicochemical Hydrodynamics: An Introduction*, Wiley, New York.

Rice, C.L. and R. Whitehead, 1965, Electrokinetic flow in a narrow cylindrical capillary, *J. Phys. Chem.* **69**, 4017.

Stone, H.A., A.D. Stroock and A. Ajdari, 2004, Engineering flows in small devices: microfluidics toward a lab-on-a-chip, *Ann. Rev. Fluid Mech.* **36**, 381.

Taylor, J.A. and E.S. Yeung, 1993, Imaging of hydrodynamic and electrokinetic flow profiles in capillaries, *Anal. Chem.* **65**, 2928.

Tretheway, D.C. and C.D. Meinhart, 2002, Apparent fluid slip at hydrophobic microchannel walls, *Phys. Fluids* **14**, L9.

Tretheway, D.C. and C.D. Meinhart, 2004, A generating mechanism for apparent fluid slip in hydrophobic microchannels, *Phys. Fluids* **16**, 1509.

Watanabe, K., Y. Udagawa and H. Udagawa, 1999, Drag reduction of Newtonian fluid in a circular pipe with highly water-repellant wall, *J. Fluid Mech.* **381**, 225.

Werner, C., H. Körber, R. Zimmermann, S. Dukhin and H.-J. Jacobasch, 1998, Extended electrokinetic characterization of flat solid surfaces, *J. Colloid Interface Sci.* **208**, 329.

Yang, C. and D. Li, 1997, Electrokinetic effects on pressure-driven liquid flows in rectangular microchannels, *J. Colloid Interface Sci.* **194**, 95.

Zhu, Y. and S. Granick, 2001, Rate-dependant slip of Newtonian liquid at smooth surfaces, *Phys. Rev. Lett.* **87**, 096105.

Zhu, Y. and S. Granick, 2002, Limits of the hydrodynamic no-slip boundary condition, *Phys. Rev. Lett.* **88**, 106102.